Energy Proceedings
Vol 49, 2024
ISSN 2004-2965

Stability analysis of a multi-terminal DC system considering the stochastic state of electric vehicles#

Yin Yi[1], Yun Zhou [1*], Ning Ma[2], Donghan Feng[1], Yuanhao Feng[1], Wenhang Yin[1]

1 Key Laboratory of Control of Power Transmission and Conversion (Ministry of Education)

Shanghai Jiao Tong University, Shanghai, China

2 State Grid Corporation of China's European Office, Berlin, Germany

ABSTRACT

The proliferation of DC charging stations is increasing steadily, and the integration of multi-terminal DC systems is a crucial prerequisite for facilitating the charging of electric vehicles with direct current. The stochastic charging state of electric vehicles present a formidable challenge to the stability of DC systems. This research focuses on a multi-terminal DC system with N electric vehicles as its primary subject. To assess the system's stability in the face of the stochastic charging state of N vehicles, a small signal stability analysis method that relies on reduced order matrixes is employed. Moreover, a novel numerical index is introduced to quantitatively evaluate the risk of instability, offering valuable insights for formulating effective charging control strategies. To validate the effectiveness of the proposed method, a nonlinear time domain model is constructed in Simulink and subjected to rigorous testing.

Keywords: multi-terminal DC system, stochastic charging state, small signal stability analysis, instability risk

NONMENCLATURE

Abbreviations	
EV	Electric vehicles
PV	Photovoltaic
ESS	Energy storage system
VSC	Voltage source converter
Symbols	
$G_{vk}(s)$	Voltage inner loop transfer function
$G_{ik}(s)$	Current outer loop transfer function
$\mathbf{X}_k$	State space model of the k^{th} EV
$\mathbf{X}_M$	State space model of the *N* EVs
P	Participation matrix of eigenvalues
$\mathbf{A}_k$	EVs state coefficient matrix
A	DC system state coefficient matrix

1. INTRODUCTION

Renewable energy's expansion drives electric vehicle (EV) demand, highlighting the imperative of studying large-scale EV integration's impact on multi-terminal DC system stability [1].

The issue of small disturbance stability in multi-terminal DC distribution systems is a prominent research topic within the field of power distribution systems [2]. In distributed scenarios with broad voltage regulation and substantial power demands, the conventional choice is droop control [3]. Conversely, for scenarios demanding high regulation precision and rapid response [4], the master-slave control scheme is typically favored. In DC systems that incorporate electric vehicles, the master-slave control mode is often preferred due to its quick response and direct control attributes.

Currently, research on the impact of EV integration on DC systems is broadly categorized into two areas. On the one hand, it is the steady-state operation optimization of EV integration, such as economic scheduling and planning [5, 6]; on the other hand, it is the dynamic analysis of EV integration, such as the analysis of the influence of the parameters of the control loop and filter loop of the EV on the stability of the DC system [7]. After detailed modeling and analysis of the EV, the results show that the control loop parameters generally have a small impact on the DC system stability, while the filtering parameters and the dynamics of the DC network have a larger impact, which is demonstrated by the eigenvalue distribution graph [8].

A major blank of the stability analysis of integrated EVs DC systems is stability analysis of a multi-terminal DC system considering stochastic EVs charging power. Therefore, methods that numerically assess the multi-terminal DC system stability under varying EVs charging power are desirable. Conventional full-order models for integrating multi-terminal DC systems for EVs are

This is a paper for the 16th International Conference on Applied Energy (ICAE2024), Sep. 1-5, 2024, Niigata, Japan.

complex. As usual, a small-signal model is only suitable for analyzing one system, which is not universal. Hence, this paper makes the following work:

Developing dynamic model of *N* EVs charging piles and full-order model of a multi-terminal DC system, which adopt the master-slave control mode. Furthermore, we propose a small-signal stability analysis method based on a reduced-order model and numerical instability risk assessment for integrated EVs DC systems. Finally, the proposed method is validated in a nonlinear time-domain model.

2. MODELING OF MULTI-TERMINAL DC SYSTEM FOR INTEGRATED ELECTRIC VEHICLES

2.1 Modelling of N EV charging piles

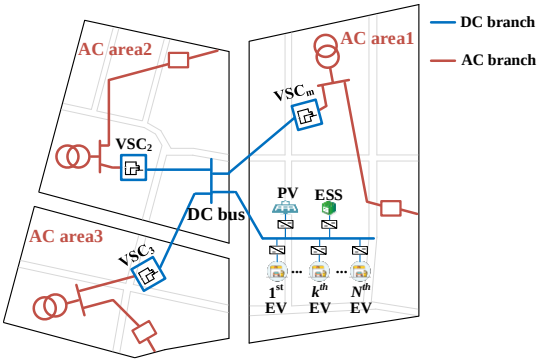

Fig. 1 Structure of the system with EVs

Fig. 1 is a schematic diagram of the multi-terminal DC system of the integrated a charging station. It includes three converter stations VSC$_m$, VSC$_2$ and VSC$_3$; photovoltaic (PV) unit, energy storage system (ESS) and *N* EV charging piles.

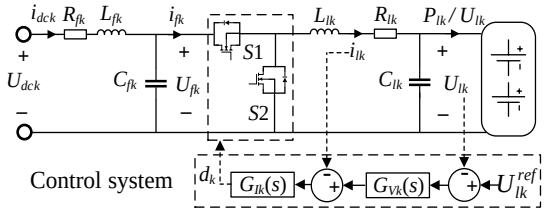

Fig. 2 Configuration of the kth EV charging pile

The circuit shown in Fig. 2 adopts double closed-loop control. $G_{vk}(s)$ is the transfer function of voltage inner loop, and $G_{ik}(s)$ is the transfer function of current outer loop.

$$G_{Vk}(s)=k_{Vpk}+\frac{k_{Vik}}{s},G_{Ik}(s)=k_{Ipk}+\frac{k_{Iik}}{s} \tag{1}$$

Combining state space modeling and small signal analysis method [4], the state space model of the k^{th} EV charging pile can be expressed as the following:

$$\frac{d\Delta\mathbf{X}_k}{dt}=\mathbf{A}_k\Delta\mathbf{X}_k+\mathbf{B}_k\Delta U_{dck},\quad \Delta i_{dck}=\mathbf{C}_k\Delta\mathbf{X}_k \tag{2}$$

where $\Delta\mathbf{X}_k=\left[i_{dck},i_{lk},U_{fk},U_{lk},\Delta x_{Ik},\Delta x_{Vk}\right]^T$.

Based on (2), the linearization of *N* EV charging piles shall be obtained as:

$$s\mathbf{X}_M=\mathbf{A}_M\mathbf{X}_M+\mathbf{B}\Delta\mathbf{U}_{dc},\Delta\mathbf{I}_{dc}=\mathbf{C}_M\mathbf{X}_M \tag{3}$$

where, $\mathbf{X}_M=[\mathbf{X}_1\ldots\mathbf{X}_N]^T$, $\Delta\mathbf{I}_{dc}=[\Delta i_{dc1}\ldots\Delta i_{dcN}]^T$, $\Delta\mathbf{U}_{dc}=[\Delta U_{dc1}\ldots\Delta U_{dcN}]^T$.

2.2 Modelling of the multi-terminal DC system with EVs

The equivalent circuit of multi-terminal DC system is shown in Fig. 3. The EV charging piles in this structure are all DC charging piles with V2G function.

The multi-terminal DC system adopts master-slave control to achieve fast power regulation. VSC$_m$ as the master station, using constant DC voltage control. The state sapce model of VSC$_m$ can be expressed as the following [4]:

$$\frac{d\Delta\mathbf{X}_m}{dt}=\mathbf{A}_m\Delta\mathbf{X}_m \tag{4}$$

VSC$_1$ and VSC$_2$ adopt constant power control, which is the slave station. The state space model of VSC converter at each constant power station can be obtained as (5).

$$\frac{d\Delta\mathbf{X}_i}{dt}=\mathbf{A}_{ni}\Delta\mathbf{X}_i+\mathbf{B}_{ni}\Delta U_i \tag{5}$$

When each slave station absorbs power from the DC network in a constant power mode, the renewable energy and ESS can be equivalent to a constant power load. The small signal model of the system can be obtained by combining the mathematical models of the above *N* EV charging piles, voltage source converter (VSC), PV and ESS, as shown in (6).

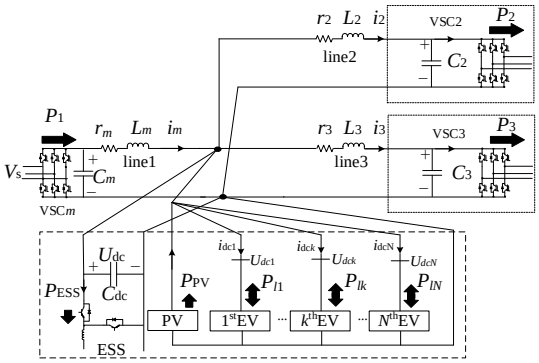

Fig. 3 Equivalent circuit of the multi-terminal DC system with EVs

$$\left[\frac{d\Delta\mathbf{X}}{dt}\right]=\mathbf{A}\left[\Delta\mathbf{X}\right]+\mathbf{B}\left[\Delta U\right] \tag{6}$$

where $\Delta\mathbf{X}=[\Delta\mathbf{X}_m\ \Delta\mathbf{X}_2\ \Delta\mathbf{X}_3\ \Delta\mathbf{X}_k\ \Delta\mathbf{U}_{dc}\ \Delta\boldsymbol{i}_{dcm}\ \Delta\boldsymbol{i}_{dc2}\ \Delta\boldsymbol{i}_{dc3}]^T$.

The above mentioned EVs state coefficient matrix $\mathbf{A}_k$ and DC system state coefficient matrix **A** are attached to the appendix.

3. STABILITY ANALYSIS OF THE DC SYSTEM CONSIDERING EV STOCHASTIC STATES

3.1 DC system stability analysis with a single EV

The distribution of eigenvalues of the system state space model reflects the stability of the system [7]. Therefore, the eigenvalues are obtained for the state space model in (6) at a value of 1 for the number of EV *N*.

Among them, the parameters of the converter station and the EV charging pile are as follows:

At a value of 1 for the number of EV *N*, eigenvalues are obtained for the state space equation shown in (6). Set the rated voltage of the master station (constant DC voltage station) as 800V, the parameters of the inner loop PI controller as K_{dm}^{p} =22.56, K_{dm}^{i} =6. The outer loop PI coefficients K_{Pm}^{p} =30, K_{Pm}^{i} =1500. The rated power of the slave station (constant power converter station) as 250kW, the parameters of the inner loop PI controller as K_{d}^{p} =22.56, K_{d}^{i} =6. The outer loop PI coefficients K_{P}^{p} =1.51, K_{P}^{i} =25. The parameters of the EV charging pile are shown as the following: the outer voltage PI controller k_{Vpk} =0.06, k_{Vik} =300; the inner current PI controller k_{Ipk} =0.2, k_{Iik} =1000.

The eigenvalue matrix is found to have a total of 31 elements, i.e., $\mathrm{Z}=[\lambda_1,\ldots,\lambda_{31}]^T$.

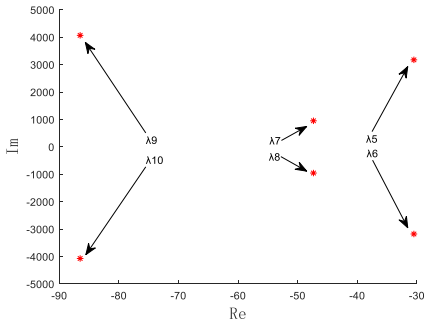

Fig. 4 EV-related eigenvalue distribution(k=1)

$$P=\begin{array}{c} \\ \Delta x_1 \\ \\ \Delta x_k \\ \\ \Delta x_n \end{array}\begin{array}{c} \begin{array}{cccccc} \lambda_1 & & \lambda_i & & \lambda_n \end{array} \\ \begin{bmatrix} u_{11}v_{11} & \cdots & u_{1i}v_{1i} & \cdots & u_{1n}v_{1n} \\ \vdots & & \vdots & & \vdots \\ u_{k1}v_{k1} & \cdots & u_{ki}v_{ki} & \cdots & u_{kn}v_{kn} \\ \vdots & & \vdots & & \vdots \\ u_{n1}v_{n1} & \cdots & u_{ni}v_{ni} & \cdots & u_{nn}v_{nn} \end{bmatrix} \end{array} \tag{7}$$

The participation factor between each eigenvalue and the state variable can be derived from (7).

To determine the relationship between state variables and modes, the participation matrix **P** is used to measure the degree of correlation between state variables and modes. The element $p_{ki}=u_{ki}v_{ki}$ of the participation matrix **P** is the participation factor, which measures the mutual participation of the i^{th} modality and the k^{th} state variable.

Table I. Participation factors of EV-related variables

Variables	λ_5	λ_6	λ_7	λ_8	λ_9	λ_{10}
Participation factor p	0.33 5+0i	0.70 6+0i	0.17 3+0i	0.28 4+0i	0.34 5+0i	0.16 7+0i

According to the correspondence between the participation factors and the coefficient matrix **A**, the participation factors of the state variables related to EV are obtained as shown in Table I. Therefore, the eigenvalues associated with EV are λ_5, λ_6, λ_7, λ_8, λ_9 and λ_{10} in **Z**. Its distribution is shown in Fig. 4. All are on the left side of the origin. By Lyapunov's first theorem, the DC system is stable at this time.

3.2 DC system stability analysis with N EVs

From $\mathbf{A}_k$ in the appendix, it is known that the affecting factors are line parameters, controller parameters and EV charging power. In engineering, for a DC system with a certain structure, the line parameters and controller parameters are basically constant. Considering that the charging power of each EV is variable, the main change of the coefficient matrix $\mathbf{A}_k$ is caused by the charging power. Therefore, the number of variables when *N* vehicles are charged is *N*. The charging power boundary is defined as $P_{\min}\le P_{lk}\le P_{\max}$. $P_{\min}$ and $P_{\max}$ the minimum and maximum power of charging power of EV charging pile respectively. Then the charging power of the k^{th} car can be expressed as (8):

$$P_{lk}=P_{\min}+\Delta P_k=P_{\max}-(P_{dif}-\Delta P_k) \tag{8}$$

where $P_{\text{dif}}=P_{\max}-P_{\min}$. ΔP_k is the increment of charging power from $P_{\min}$, k=1,2,…,N.

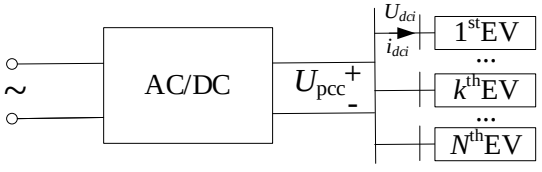

Fig. 5 Two-port simplified network of DC system

At this time, the charging power is considered to be an important factor affecting the **A**. Different charging

power values correspond to different coefficient matrices. $P_{\min}, P_{\max}, \Delta P_k$ and P_{dif} correspond to $\mathbf{A}_{\min}$, $\mathbf{A}_{\max}$, $\mathbf{A}_{pk}$ and $\mathbf{A}_{dif}$. The following relationships exist:

$$\mathbf{A}_k = \mathbf{A}_{\min} + \mathbf{A}_{pk} = \mathbf{A}_{\max} - (\mathbf{A}_{dif} - \mathbf{A}_{pk}) \tag{9}$$

At this time, if the multi-terminal DC system in Fig. 3 is simplified to a two-port network, there is $\Delta U_{\text{pcc}} = 0$. From this, the following equation can be obtained:

$$\Delta \mathbf{U}_{\mathbf{dc}} = -\mathbf{Z}(j\omega)\Delta \mathbf{I}_{dc} \tag{10}$$

When $\omega = \omega_0$, $\mathbf{Z}(j\omega_0)$ is simplified to **Z**. Combined with (3), **A** matrix can be expressed as:

$$\begin{aligned} \mathbf{A} &= \mathbf{A}_M - \mathbf{B}_M \mathbf{Z} \mathbf{C}_M \\ &= diag(\mathbf{A}_k) - [\mathbf{Z} \otimes \mathbf{I}] diag(\mathbf{B}_k \mathbf{C}_k) \end{aligned} \tag{11}$$

where **I** is a 6*6 matrix. $\mathbf{Z} \otimes \mathbf{I}$ means the kronecker product between **Z** and **I**.

Equation (11) is obtained immediately by coupling with (9):

$$\begin{aligned} \mathbf{A} &= diag(\mathbf{A}_{\min}) + diag(\mathbf{A}_{pk}) - [\mathbf{Z} \otimes \mathbf{I}] diag(\mathbf{B}_k \mathbf{C}_k) \\ &= diag(\mathbf{A}_{\max}) - diag(\mathbf{A}_{dif} - \mathbf{A}_{pk}) \\ &\quad - [\mathbf{Z} \otimes \mathbf{I}] diag(\mathbf{B}_k \mathbf{C}_k) \end{aligned} \tag{12}$$

The similarity transformation in (12) can be obtained by substituting the similarity transformation in [9]:

$$\begin{aligned} \mathbf{P}\mathbf{A}\mathbf{P}^{-1} &= diag(\mathbf{A}_{\min}) - diag(\lambda_k \mathbf{I}) diag(\mathbf{B}_k \mathbf{C}_k) \\ &\quad + \mathbf{P} diag(\mathbf{A}_{pk}) \mathbf{P}^{-1} \\ &= diag(\mathbf{A}_{\max}) - diag(\lambda_k \mathbf{I}) diag(\mathbf{B}_k \mathbf{C}_k) \\ &\quad - \mathbf{P} diag(\mathbf{A}_{dif} - \mathbf{A}_{pk}) \mathbf{P}^{-1} \end{aligned} \tag{13}$$

The stability of the DC system can be judged by the eigenvalue stability region method mentioned in [10] with (13). From this theory, the following conclusions can be drawn:

The eigenvalue vector of the DC system coefficient matrix **A** considering *N* electric vehicles is $\lambda_{dk} = [\lambda_{d1k} \ldots \lambda_{d6k}]^T$. The following relations can be obtained:

$$\text{Re}(\lambda_{\min k}) \le \text{Re}(\lambda_{dk}) \le \text{Re}(\lambda_{\max k}) \tag{14}$$

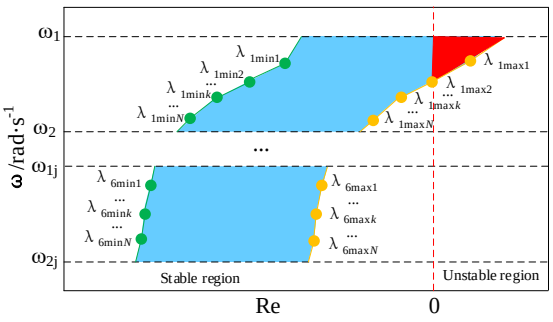

Fig. 6 Diagram of the DC system stable region

From (14), the diagram of stability region of DC system can be obtained. In Fig. 6, the stability region of the DC system with *N* electric vehicles at different frequencies is shown. The green curve is the curve formed by $\lambda_{\min k}$, and the yellow curve is the curve formed by $\lambda_{\max k}$. The enclosed area is the possible area of the eigenvalue of the DC system. According to the first method of Lyapunov, the left half of the imaginary axis is divided into a stable region. Therefore, the blue area in Fig. 6 is the stable area of the DC system with *N* EVs, and the red area is the unstable area. When the charging power of the DC system P_{lk} is uniformly distributed at [$P_{\min}$, $P_{\max}$], its instability can be evaluated numerically.

$$D_a = \frac{S_{unstable}}{S_{unstable+stable}} (\omega_{1j}, \omega_{2j}) \tag{15}$$

where $S_{unstable}$ is the number of eigenvalues of the DC system in the unstable region when ω in (ω_{1j}, ω_{2j}). $S_{unstable+stable}$ is the total number of eigenvalues of DC system in stable region and unstable region.

When the left boundary is on the right side of the imaginary axis, the risk of the DC system D_a = 100 %. Conversely, when the right boundary is on the left side of the imaginary axis, the risk of the DC system D_a = 0%, indicating that the DC system is unstable at this time.

Considering specific power limits, such as $P_{\min 1k}$=20 kW and $P_{\max 1k}$=40 kW, it is possible to derive eigenvalues, including λ_k, $\lambda_{\min 1k}$, $\lambda_{\max 1k}$, λ_{d1k} based on the aforementioned DC system parameters. Subsequently, the stability region of the DC system can be determined by evaluating the region defined by $\lambda_{\min 1k}$ and $\lambda_{\max 1k}$ across four distinct oscillation modes. In the oscillation mode, it contains all the results of the oscillation calculation of the DC system under the current parameters. It can be seen from Fig. 7 that the right boundaries of all blue regions are in the left half of the imaginary axis. Therefore, the DC system is stable in these oscillation modes. D_{a1}=D_{a2}=D_{a3}=D_{a4}=0, the risk of instability is 0.

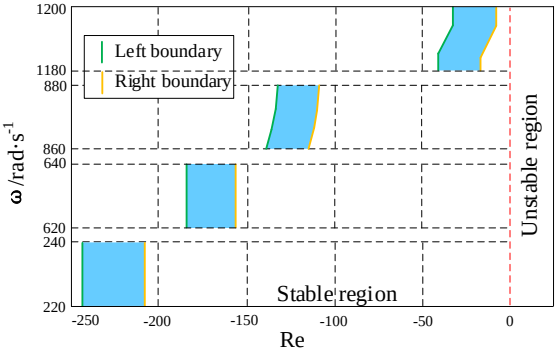

Fig. 7 Stable region of the DC system ($P_{\min 1k}$=20kW, $P_{\max 1k}$=40kW)

Moreover, the stability of the DC system after changing the charging power of the EV is shown in Fig. 8. Taking ω in (860,880) rad/s of Fig. 7 as the research

object, the P_{min1k} in this oscillation mode is increased by 10 kW, and its state is shown in region a in Fig. 8. The area of the blue area increases, and the right boundary intersects with the imaginary axis. The DC system exists instability risk, and its risk coefficient D_{a3}=2.7%. Furthermore, the eigenvalue distribution of the DC system when P_{min1k} is increased from 20kW to 25kW is shown in the b region of Fig. 8. The left boundary moves to the right boundary, and the blue area narrows. The instability risk of the DC system is D_{a3}=4.1%.

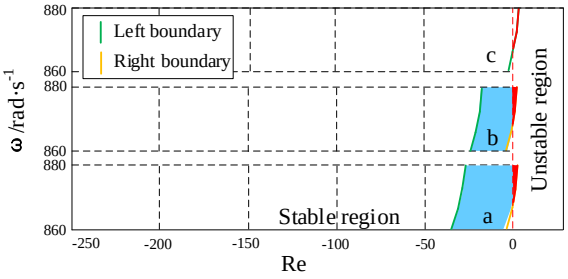

Fig. 8 Stable region of the DC system when the EV charging power changes

If P_{min1k} = P_{max1k} =60kW, the calculated eigenvalue distribution of the DC system is shown in region c in Fig. 8. At this time, the left boundary and the right boundary overlap, and both intersect with the imaginary axis. The instability risk of the DC system is D_{a3}=100 %. This shows that the instability risk of EVs running at the maximum charging power is the largest. In this case, in order to ensure the stability of the DC system when the EV is stochastically charged, the maximum charging power of the charging pile should not exceed 60 kW.

4. SIMULATION VERIFICATION

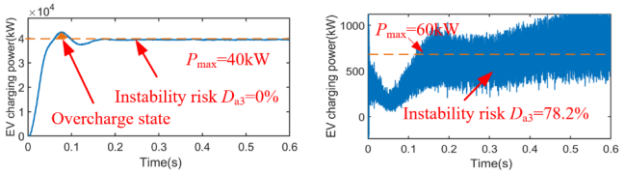

Fig. 9 EV charging power when P_{max} of EVs changes

In order to verify the above analysis method, the corresponding nonlinear time domain simulation model is established in Simulink for verification (N=6). Fig. 9 shows the curve of P_{max} with a changing from 40kW to 60kW. Meanwhile, P_{min} remain unchanged at 20kW. Taking ω in (860,880) rad/s of Fig. 7 as the research object, the left diagram is the power curve of the EV charging pile with P_{max}=40kW, and 2% overcharge occurs. The instability risk D_{a3}=0%, obtained by (15). The right diagram is the state when P_{max}=60kW. This curve shows a diffusion oscillation phenomenon, the instability risk D_{a3}=78.2%, and the DC system is in an unstable state.

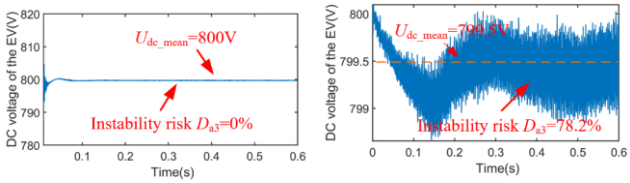

Fig. 10 DC voltage of when P_{max} of EVs changes

Furthermore, the DC voltage also shows the same trend in Fig. 10. When P_{max} =40kW, the voltage is stable and the risk of instability is D_{a3}=0%. While P_{max} changes to 60kW, the voltage diffusion oscillation occurs due to the output exceeding the margin, and the instability risk D_{a3}=78.2%.

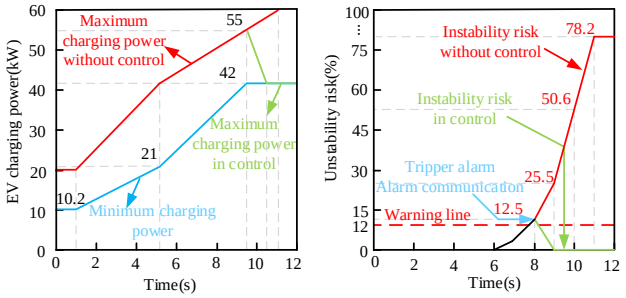

Fig. 11 Curve of the EV maximum and minimum charging power and the corresponding instability risk

Fig. 11 shows the maximum and minimum charging power curves detected for all EVs during 0-12s, and the charging power of other EVs is stochastically distributed among them. In the oscillation mode of ω in (860,880) rad/s, when P_{min} =21kW and P_{max} =42kW at 5s, it can be seen from the right diagram that the instability risk D_{a3}=0%. Hence, the DC system is in a stable state. Meanwhile, D_{a3}=12% is set as the warning line, and alarm information is sent out at 8s. The P_{max} increases to 55 kW at 9.5s. Currently, the instability risk is D_{a3}=42.3%, the DC system is unstable. If control is taken at this time, such as limiting P_{min} = P_{max} =42kW, the risk of instability can be reduced, as shown in the green curve in Fig. 11. If without control, P_{max} =60kW at 12 s, the instability risk D_{a3}=78.2%, resulting in the unstable DC system. Operators can control according to risk alerts to avoid instability risks caused by integrated EVs to the DC system.

5. CONCLUSION

This paper simulates the operation of multi-terminal DC system with integrated a charging station. The stability of the DC system under the stochastic charging state of the EV is analyzed. The main conclusions are as follows:

1) Utilizing a reduced-order small-signal methodology, the study theoretically characterizes the stability of a multi-terminal DC system experiencing stochastic charging from multiple EVs.

2) A numerical approach is introduced for appraising the instability risk associated with DC systems exposed to the EV stochastic charging state, offering valuable insights for enhancing the control and stability of the DC system.

The theoretical insights and proposed methodologies outlined above are subsequently validated through the utilization of a nonlinear time domain model within Simulink.

REFERENCE

[1] B. Zhou, T. Littler and L. Meegahapola. Assessment of transient stability support for electric vehicle integration, 2016 IEEE Power and Energy Society General Meeting (PESGM), Boston, MA, USA, 2016, pp. 1-5.

[2] T. Odun-Ayo and M. L. Crow. Structure-preserved power system transient stability using stochastic energy functions, IEEE Transactions on Power Systems, 2012,27(3): pp. 1450-1458.

[3] X. Meng, J. Liu and Z. Liu. A generalized droop control for grid-supporting inverter based on comparison between traditional droop control and virtual synchronous generator control, IEEE Transactions on Power Electronics, 2019,34(6): pp. 5416-5438.

[4] Q. Fu, W. Du, H. Wang, et al. Small-signal stability analysis of a VSC-MTDC system for investigating DC voltage oscillation, IEEE Transactions on Power Systems, 2021,36(6): pp. 5081-5091, Nov. 2021.

[5] W. Yao, et al. A multi-objective collaborative planning strategy for integrated power distribution and electric vehicle charging systems, IEEE Transactions on Power Systems, 2014,29(4): pp. 1811-1821.

[6] G. Wang et al. Robust planning of electric vehicle charging facilities with an advanced evaluation method, IEEE Transactions on Industrial Informatics, 2018,14(3): pp. 866-876, March 2018.

[7] W. Du, Q. Fu and H. F. Wang. Small-signal stability of a DC network planned for electric vehicle charging, IEEE Transactions on Smart Grid, 2020,11(5): pp. 3748-3762.

[8] W. Du, J. Zhang, Y. Zhang. Stability criterion for cascaded system with constant power load, IEEE Transactions on Power Electronics, 2013,28(4): pp. 1843-1851.

[9] M. Wu and D. D. -C. Lu. A novel stabilization method of LC input filter with constant power loads without load performance compromise in DC microgrids, IEEE Transactions on Industrial Electronics, 2015,62(7): pp. 4552-4562.

[10] M. Tabari and A. Yazdani. A mathematical model for a stability-enhanced DC distribution system for power system integration of plug-in electric vehicles, 2016 IEEE Power and Energy Society General Meeting (PESGM), Boston, MA, USA, 2016, pp. 1-5.

APPENDIX

$$\mathbf{A}_k = \begin{bmatrix} \frac{-R_{fk}}{L_{fk}} & 0 & \frac{-1}{L_{fk}} & 0 & 0 & 0 \\ 0 & \frac{-\left(R_{lk}+U_{fk0}k_{Ipk}\right)}{L_{lk}} & \frac{d_{lk0}}{L_{lk}} & \frac{-1-U_{fk0}k_{Ipk}k_{Vpk}}{L_{lk}} & \frac{U_{fk0}}{L_{lk}} & \frac{U_{fk0}k_{Ipk}}{L_{lk}} \\ \frac{1}{C_{fk}} & \frac{i_{lk0}k_{ipk}-d_{k0}}{C_{fk}} & 0 & \frac{i_{lk0}k_{ipk}k_{vpk}}{C_{fk}} & \frac{-i_{lk0}}{C_{fk}} & \frac{-i_{lk0}k_{ipk}}{C_{fk}} \\ 0 & \frac{1}{Cfk} & 0 & \frac{P_{lk}}{C_{lk}U_{lk0}{}^2} & 0 & 0 \\ 0 & -k_{Iik} & 0 & -k_{Iik}k_{Vpk} & 0 & k_{Iik} \\ 0 & 0 & 0 & -k_{Vik} & 0 & 0 \end{bmatrix}$$

$$\mathbf{A} = \begin{bmatrix} \mathbf{A}_{m(7\times7)} & 0_{(7\times7)} & 0_{(7\times7)} & 0_{(7\times6N)} & 0_{(7\times1)} & -\frac{1}{C_m} & 0_{(7\times1)} & 0_{(7\times1)} \\ 0_{(7\times7)} & \mathbf{A}_{n2(7\times7)} & 0_{(7\times7)} & 0_{(7\times6N)} & 0_{(7\times1)} & 0_{(7\times1)} & -\frac{1}{C_2} & 0_{(7\times1)} \\ 0_{(7\times7)} & 0_{(7\times7)} & \mathbf{A}_{n2(7\times7)} & 0_{(7\times6N)} & 0_{(7\times1)} & 0_{(7\times1)} & 0_{(7\times1)} & -\frac{1}{C_3} \\ 0_{(6N\times7)} & 0_{(6N\times7)} & 0_{(6N\times7)} & \mathbf{A}_{k(6N\times6N)} & 0_{(6N\times1)} & 0_{(6N\times1)} & 0_{(6N\times1)} & 0_{(6N\times1)} \\ 0_{(1\times7)} & 0_{(1\times7)} & 0_{(1\times7)} & 0_{(1\times6N)} & \frac{P_{ESS}+P_{PV}-\sum_{k=1}^{N}P_{lk}}{C_{dc}\cdot U_{dc0}} & \frac{1}{C_{dc}} & \frac{1}{C_{dc}} & \frac{1}{C_{dc}} \\ \left[\frac{1}{L_m},0_{(1\times6)}\right] & 0_{(1\times7)} & 0_{(1\times7)} & 0_{(1\times6N)} & -\frac{1}{L_m} & -\frac{r_m}{L_m} & 0 & 0 \\ 0_{(1\times7)} & \left[\frac{1}{L_2},0_{(1\times6)}\right] & 0_{(1\times7)} & 0_{(1\times6N)} & -\frac{1}{L_2} & 0 & -\frac{r_2}{L_2} & 0 \\ 0_{(1\times7)} & 0_{(1\times7)} & \left[\frac{1}{L_3},0_{(1\times6)}\right] & 0_{(1\times6N)} & -\frac{1}{L_3} & 0 & 0 & -\frac{r_3}{L_3} \end{bmatrix}$$